A Novel Hybrid Variable Stiffness Mechanism: Synergistic Integration of Layer Jamming and Shape Memory Polymer

Wenkai Yu, Jingyi Liu, Xin Li, Ziyue Yu, and Hongyan Yuan

***Abstract*—Soft robots have garnered considerable attention recently due to their versatility, compliance, and myriad applications. However, the inherent low stiffness of soft robots also limits their stability and force output capability. Hence, variable stiffness technology has emerged as a solution, which enables soft robots to modulate stiffness according to the application scenario. Two primary methods have been developed to regulate stiffness: material phase transition (MPT) based method and geometric reconfiguration (GR) based method. However, these approaches have not achieved miniaturization while maintaining a wide range of stiffness change. This work introduces a novel hybrid variable stiffness (HVS) concept that combines the MPT-based and GR-based variable stiffness methods for the first time. Specially, the HVS structure leverages shape memory polymer (SMP) method and layer jamming (LJ) to get a simultaneous response. Bending tests reveal that the compact bi-layer designed HVS structure can achieve a wide stiffness range (0.31 N/mm $\sim$ 4.86 N/mm, 15.7 times) and load-bearing capacity (1.76 N$\sim$ 28.1 N, 16.0 times), which has been simulated by finite element analysis. Response tests show that the jamming response is rapid ($\sim$ms) while the maximum heating rate is 2.77 $\pm$ 0.16 °C/s, indicating that the HVS structure can achieve a relatively fast response. Furthermore, a soft gripper equipped with the HVS structure is developed to illustrate the enhanced grasping ability. Several performed grasping tests reveal that the variable stiffness soft gripper can grasp various objects with diverse shapes (40.0 mm $\sim$ 190 mm, 4.75 times) and materials while lifting a weight up to 650 g, which provides an effective solution for the complex application requirements of soft robots.**

***Index Terms*—Soft robots, hybrid variable stiffness, layer jamming, shape memory polymer, gripper.**

I. Introduction

SOFT robotics, an emerging field of robots that has received widespread attention in recent decades, represents the frontier of advanced robotics research [1]. Soft robots can mimic unique soft biological organs or animal mechanisms in nature, such as octopus tentacles, elephant trunks, or snake locomotion [2], [3], [4]. Unlike traditional rigid robots, soft robots are fabricated of soft materials with low modulus, such as silicone rubber, hydrogel, and dielectric elastomers that can undergo large strains or rotations. With superior compliance, soft robots can generate continuous large deformations and contact with the environment closely without causing damage [5], [6], [7], rendering them highly safe for human-robot interaction and particularly suitable for unstructured environments, e.g., inspection, medical and rehabilitation, haptic devices, etc.

However, the inherent lower stiffness of soft robots concomitantly engenders poor stability, anti-interference ability, and limited force output ability, posing new challenges to their applications [8], [9]. To address the limitations, variable stiffness technology has emerged as a solution, which enables robots to modify their stiffness according to the application scenario. It has been widely adopted in broad fields such as grippers [9], [10], [11], [12], [13], aircraft landing gear [14], medical endoscopes [15], [16], artificial skin [17], and promising deployable buildings [18].

The stiffness of soft robots depends on two principal factors, the Young's modulus of the material, and the geometric shape parameters. The relationship between stiffness and the two factors is positively correlated. Accordingly, current methods for regulating stiffness can be classified into two approaches. The first approach exploits material phase transition (MPT) to modify Young's modulus and thereby regulate stiffness. The second approach leverages geometric reconfiguration (GR) to modify equivalent geometric shape parameters of robots and thus regulate stiffness. Each approach can independently adjust stiffness and has its unique advantages and disadvantages contingent on specific application requirements.

The MPT-based variable stiffness concept leverages smart materials that can respond to external stimuli. According to the type of material, there are several available options, including shape memory alloy/polymer (SMA/SMP) [12], [19], [20], low melting point alloys (LMPA) [15], [16], [21], electrorheological/ magnetorheological fluids (ER/MR) [22], and other smart chemical materials [23]. While the MPT-based variable stiffness concept is highly dependent on material properties. SMA/SMP and LMPA are challenging to miniaturize while retaining high stiffness. The Joule heating stimuli will also introduce significant thermal effects. The ER/MR have simple and fast stimuli and

Manuscript received 29 August 2023; accepted 12 January 2024. Date of publication 22 January 2024; date of current version 9 February 2024. This letter was recommended for publication by Associate Editor N. Gravish and Editor Y. L. Park upon evaluation of the reviewers' comments. This work was supported in part by the National Natural Science Foundation of China under Grant 12072143, and in part by the Science, Technology and Innovation Commission of Shenzhen Municipality under Grant ZDSYS20210623092005017. *(Corresponding author: Hongyan Yuan.)*

The authors are with the Shenzhen Key Laboratory of Soft Mechanics and Smart Manufacturing, Department of Mechanics and Aerospace Engineering, Southern University of Science and Technology, Shenzhen 518055, China (e-mail: 12031088@mail.sustech.edu.cn; 12331112@mail.sustech.edu.cn; 12031016@mail.sustech.edu.cn; 12011017@mail.sustech.edu.cn; yuanhy3@sustech.edu.cn).

This letter has supplementary downloadable material available at https://doi.org/10.1109/LRA.2024.3357035, provided by the authors.

Digital Object Identifier 10.1109/LRA.2024.3357035

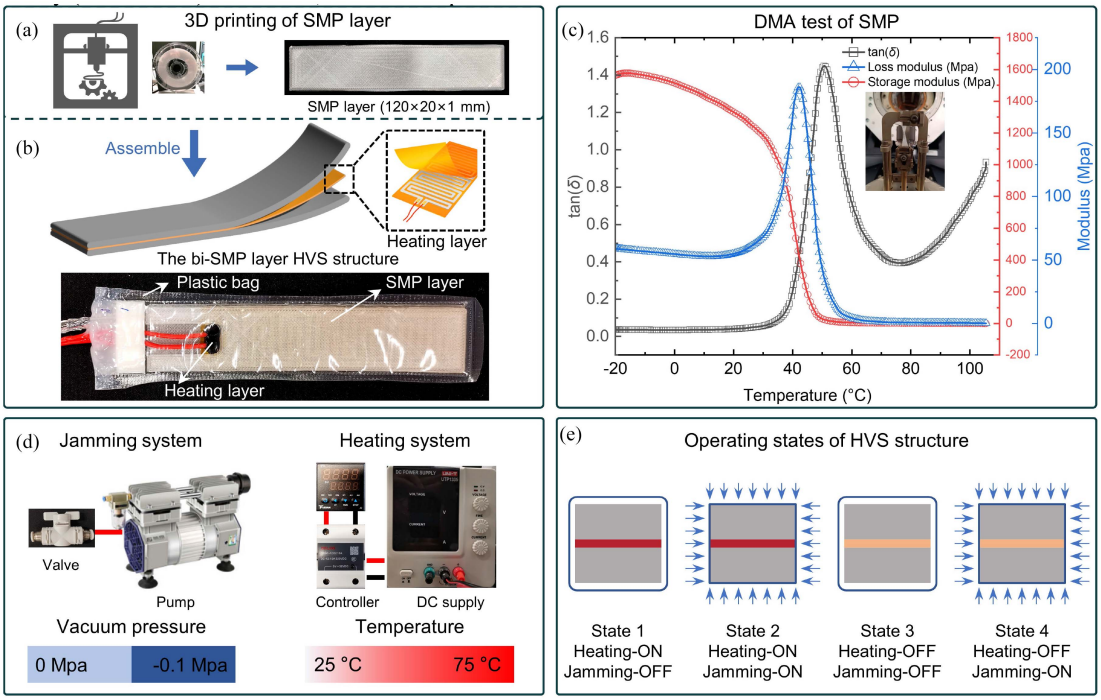

Fig. 1. Design, fabrication, and actuation of the Hybrid Variable Stiffness (HVS) structure. (a) Shape-memory polymer (SMP) layer and 3D printing process. (b) Schematics and prototype of the HVS structure. (c) Dynamic mechanical analysis results of the SMP. (d) The dual-stimuli through jamming and heating systems. (e) The operating states of the HVS structure.

response. But it has limited stiffness range and their actuation requires relatively bulky field-generating equipment, constraining their widespread applications.

GR-based variable stiffness approaches include jamming, metamaterials [24], self-locking structures [11], counteract structures [25], and other mechanical designs. GR-based approaches enable rapid response but commonly have structural redundancy and large volumes. Among them, jamming is the most common method, typically comprising two components: a jamming structure composed of small-sized particles (Particle/Granular Jamming, PJ/GJ) [26], [27], [28], [29], fibers (Fiber Jamming, FJ) [28], [30], [31], or layers (Layer/Laminar Jamming, LJ) [10], [17], [32], [33], [34], and an actuation system that capable of regulating the internal mutual forces. The internal mutual forces (e.g., electrostatic adhesive or frictional forces) increase rapidly under actuation, rigidizing the loose structure and effectively increasing the equivalent structural geometric parameters and stiffness. Jamming-based variable stiffness mechanism enables fast response (ms) but requires a large number of interfering objects to achieve high stiffness, resulting in bulky, functional redundant mechanisms since the structures lack tunable material properties.

We conducted a comprehensive literature review of the existing variable stiffness methods, including stimuli, maximum/minimum stiffness, and response time, as summarized in Table I. Current variable stiffness concepts have not achieved miniaturization and rapid response while maintaining a wide stiffness range, substantially limiting application in miniaturized, high-precision soft robots. Consequently, there is an urgent need for a variable stiffness structure with a small size but a wide range of stiffness change, easy manufacturing, and simple assembling. This paper presents a novel hybrid variable stiffness (HVS) mechanism that integrates the MPT-based and GR-based concepts (i.e., the SMP and LJ), which enables the simultaneous modulation of Young's modulus and the geometric structure parameters to achieve the desired stiffness. This provides an effective solution for the complex demands of soft robot applications. To the best of our knowledge, the proposed hybrid variable stiffness mechanism integrates the two different variable stiffness concepts for the first time and shows great potential. A soft gripper incorporating the HVS structure will be developed to verify its effectiveness. Grasping experiments with various objects will demonstrate its interactive, secure, and flexible nature as well as its stable grasping and force output capability under high stiffness states.

II. Development of the Hybrid Variable Stiffness (HVS) Mechanism

A. Design and Fabrication of the HVS Structure

To validate the proposed hybrid variable stiffness (HVS) mechanism systematically, shape memory polymer (SMP) and layer jamming (LJ) are adopted as the implementation method. The prototype of the sandwich-shaped HVS structure is shown in Fig. 1(a). The components and fabrication process are as follows: The commercial 4D printing SMP consumables (Gen 7, Kangxun Co., LTD.) were utilized to fabricate the SMP layers ($120 \times 20 \times 1$ mm) via 3D printing (Ender-5, Creality Co., LTD.). The primary printing process parameters are listed in Table II. The commercial polyimide heating layer ($100 \times 20 \times$

TABLE I
SUMMARY OF THE VARIABLE STIFFNESS MECHANISM AND ITS PERFORMANCE

Ref	Mechanism		Stimuli	Stiffness			Response time
	GR	MPT		Min	Max	Ratio	
[30]	FJ	-	Vacuum	-	~4.7 N/mm	0.2	ms
[33]	LJ	-	Vacuum	-	-	5	ms
[10]	LJ	-	Voltage	-	-	7	ms
[17]	LJ	-	Vacuum	0.67 N/mm	31.05 N/mm	47	ms
[27]	PJ	-	Vacuum	0.559 N/mm	5.045 N/mm	9.02	ms
[35]	PJ	-	Vacuum	12.5 KPa	61.3 KPa	5	ms
[28]	PJ/LJ	-	Vacuum	0.006 N/mm	0.033 N/mm	5.52	ms
[11]	Self-locking	-	Motor	-	-	20	ms
[36]	Friction	-	SMA	-	0.035 N/mm	3	-
[37]	-	ER	Voltage	42 N/m	622 N/m	14.8	ms
[38]	-	LMPA	Joule heating	-	3 Gpa	-	10 s
[39]	-	LMPA	Joule heating	0.1 Mpa	1.8 Mpa	18	-
[40]	-	LMPA	Joule heating	4.5 Mpa	1253.6 Mpa	278	16 s
[41]	-	Polymer	Joule heating	0.47 Mpa	22.22 Mpa	47	35 s
[42]	-	Polymer	Joule heating	0.057 N/mm	1.484 N/mm	25	82 s
[23]	-	Material	Ethanol	0.51 MPa	243.6 Mpa	477	2.5 h
[20]	-	SMP	Joule heating	0.035 N/mm	0.181 N/mm	5	86 s
[43]	-	SMP	Joule heating	0.062 GPa	2.3 GPa	37.2	485 s
[12]	-	SMP	Joule heating	16 mN/mm	288 mN/mm	120	32 s
[44]	-	SMP	Joule heating	11 mN/mm	572 mN/mm	52	-
[19]	-	SMP	Joule heating	2.31 MPa	128.48 MPa	55	275 s
This work	LJ	SMP	Vacuum/ Joule heating	0.31 N/mm	4.86 N/mm	15.7	ms/16 s

- Not mentioned in reference

TABLE II
3D PRINTING PROCESS PARAMETERS OF SMP LAYER

Parameters	Value
Speed	50 mm/s
Layer thickness	0.1 mm
Bed temperature	55 °C
Nozzle temperature	215 °C
Density	100%

0.25 mm, Rebainian Co., LTD.) is positioned between two SMP layers. After assembly, the HVS structure was sealed in a plastic bag (polyethylene, PE). The wires of the heating layer and the vacuum tube pass through the reserved holes of the plug and are connected to the heating and jamming system respectively. The plug and the end of the plastic bag are finally sealed with liquid silicone glue.

The HVS structure has two independent stimuli (Joule heating and vacuum pressure), which can be realized by the designed heating and jamming systems, as shown in Fig. 1(d). The heating system includes a heating layer, a temperature sensor (K-type thermocouple), a temperature controller, a relay, and a direct current (DC) power supply. The temperature sensor is attached to the external surface of the plastic bag and connected to the temperature controller. After measuring the temperature, the controller compares it with the predetermined setpoint and controls the on-off of the heating layer by the relay. With the designed heating system, the temperature can be continuously regulated between 25 °C and 75 °C, with a control accuracy of 0.1 °C. The jamming system consists of an air pump and a valve, which is relatively simple. The air tube is directly connected to the air pump, and the jamming is achieved by switching the working states of the valve. Due to the considerable flow and velocity of the vacuum pump and the limited amount of air inside the sealing bag, the HVS structure can be evacuated to vacuum (−0.1 Mpa) instantaneously (within 1 ms). Therefore, the vacuum pressure can be regulated to 0 or −0.1 Mpa. The hybrid operating states can be classified into four classes with different stimuli, as shown in Fig. 1(e) and Table III.

TABLE III
THE OPERATING STATES OF THE HVS STRUCTURE

State	Jamming (Vacuum pressure)	Heating (Temperature)
1	OFF (0 Mpa)	ON (25 °C ~ 75 °C)
2	ON (-0.1 Mpa)	ON (25 °C ~ 75 °C)
3	OFF (0 Mpa)	OFF (25 °C)
4	ON (-0.1 Mpa)	OFF (25 °C)

B. Characterization of the Mechanical Properties of SMP

The thermomechanical properties of the shape memory polymer (SMP) determine the material phase transition behavior of the HVS mechanism, which is a crucial factor for further analysis. Thus, a dynamic mechanical analysis (DMA) test was performed based on the DMA 850 (TA Instrument Inc). The SMP specimen is fabricated in a film type (30 × 6 × 1 mm). The temperature increased incrementally from −20 °C to 120 °C with a rate of 5 °C min^{-1}. The DMA experimental results reveal that the storage modulus (representative of the elastic response) increases substantially from 2.8 Mpa at high temperatures (>70 °C) to more than 1260 MPa at room temperature (∼25 °C), as shown in Fig. 1(c). Besides, Young's modulus and the storage modulus is quite similar, assuming that the SMP is a linear, isotropic, and elastic material under small deformations and low temperature. Furthermore, the glass transition temperature (Tg) can be approximated to be around 50 °C, as inferred from the maximum point of the curve of loss tangent ($tan(\delta)$), which represents the ratio of the loss modulus to the storage modulus.

C. Characterization of the Frictional Properties of SMP

The frictional properties of the SMP layer are another crucial factor of the HVS mechanism, which determines the jamming behavior and the interlayer slippage. To accurately model the

TABLE IV
THE DYNAMIC FRICTION COEFFICIENTS BETWEEN SMP LAYER AND MATERIALS

	SMP
PP	1.68 ± 0.07
PDMS	2.26 ± 0.18
Steel	0.76 ± 0.09

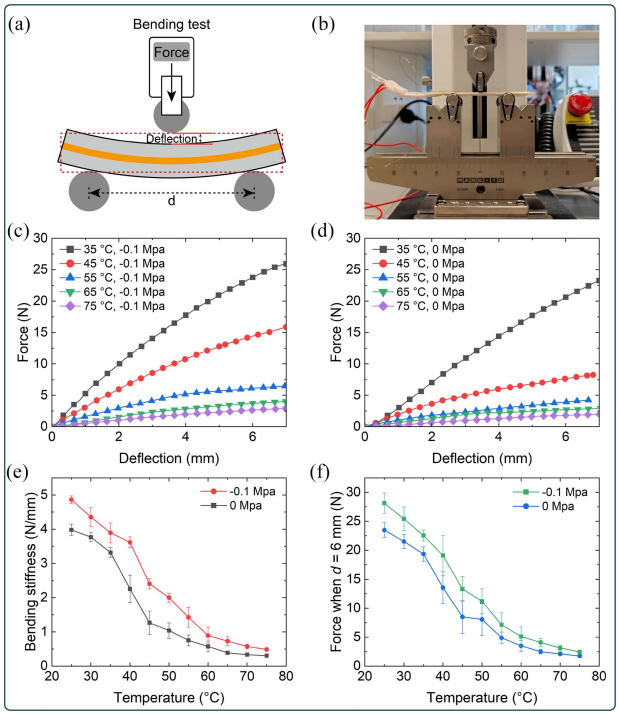

Fig. 2. Three-point bending test of the HVS structure. (a) Test illustration. (b) Experimental platform. (c) Force-deflection curves with vacuum pressure. (d) Force-deflection curves without vacuum pressure. (e) Bending stiffness at different temperatures. (f) Force output with a 6 mm deflection.

interlayer friction, the dynamic friction coefficients between the SMP layer and various materials (Polypropylene (PP), Polydimethylsiloxane (PDMS), and 304 stainless steel) are measured based on the Tribometer platform (TRB³, Anton Paar Inc), as shown in Table IV.

III. STUDY OF THE HVS MECHANISM PERFORMANCE

A. The Bending Stiffness and Load-Bearing Capacity

The bending stiffness is the primary performance parameter of the HVS structure, which reflects the ability to withstand bending moment. The load-bearing capacity is another important performance parameter of the HVS structure, which reflects the maximum force that the structure can withstand or output. To quantitatively determine these parameters of the HVS structure under different operating states, a three-point bending test was conducted based on the force measurement platform (ESM303, Mark-10), as shown in Fig. 2(a) and (b). The experimental parameters are listed as follows: the supporting span d of 48 mm, a loading rate of 10 mm/min, and a total deflection of 7 mm. The curve of loading force and deflection can be obtained

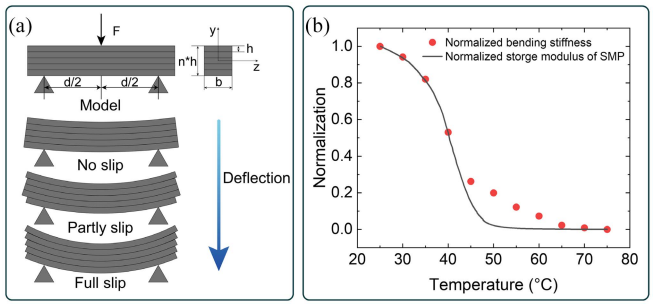

Fig. 3. Theoretical model of the HVS structure. (a) The interlayer slippage increases with the deflection. (b) The normalized bending stiffness without vacuum pressure and the normalized storage modulus of SMP.

via the bending experiments, where the curve slope represents the bending stiffness; the force magnitude under the deflection of 6 mm represents the load-bearing capacity.

According to the bending test results, the HVS structure can achieve a wide range of bending stiffness, as shown in Fig. 2(e). The minimum stiffness (0.31 ± 0.013 N/mm) occurs under State 1 (75 °C, 0 Mpa). The maximum stiffness (4.86 ± 0.11 N/mm) occurs under State 4 (25 °C, −0.1 Mpa), which is 15.7 times the minimum stiffness. Meanwhile, the HVS structure can also achieve a wide range load-bearing capacity, as shown in Fig. 2(f). The minimum force (1.76 ± 0.21 N) occurs under State 1 (75 °C, 0 Mpa). The maximum force (28.1 ± 1.76 N) occurs under State 4 (25 °C, −0.1 Mpa), which is 16.0 times the minimum force, indicating that the HVS structure can achieve a wide range of force output capacity. As the temperature decreases, the bending stiffness and the load-bearing capacity increase rapidly. Meanwhile, jamming also has a significant impact on the HVS structure under the same temperature, where the stiffness under vacuum is 1.60 ± 0.30 times larger than under non-vacuum conditions, the load-bearing capacity under vacuum is 1.39 ± 0.15 times larger than under non-vacuum conditions.

The theoretical equation for calculating the bending stiffness of the HVS structure can be expressed as $K \propto E(T) * I(P)$. Where $E(T)$ denotes Young's modulus of SMP, which is regulated by the temperature T. $I(P)$ denotes the moment of inertia of the HVS structure, which is regulated by the vacuum pressure P. The HVS structure acts as a cohesive beam under vacuum pressure. As deflection increases, gradual interlayer slippage occurs, decreasing the $I(P)$ and stiffness, as depicted in Fig. 3(a). The process will be further studied in finite element analysis. To investigate the intricate interplay between stiffness and temperature, the experimental bending stiffness without vacuum pressure and the DMA-measured storage modulus of SMP (25 °C∼75 °C) are normalized to address the inherent substantial numerical differences, as shown in Fig. 3(b). Notably, the normalized factors fit well within the temperature range of 25 °C to 45 °C, which reveals a proportional relationship between them. Nonetheless, as the temperature transcends 45 °C, discernible discrepancies emerge, which can be attributed to the rapid attenuation of the storage modulus, coupled with the neglection of the stiffness conferred by the heating layer and the sealing plastic bag. The analytical modeling of the HVS structure will be studied in future work.

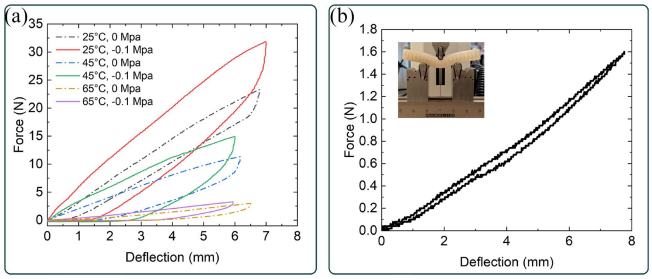

Fig. 4. Hysteresis characterization. (a) The HVS structure. (b) Soft finger.

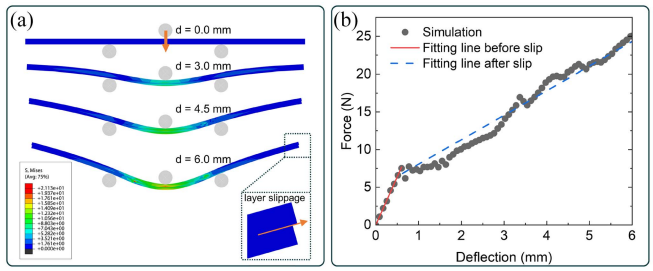

Fig. 5. Simulation of the bending of HVS structure. (a) The stress contour with different deflection. (b) The force-deflection curve and fitting stiffness.

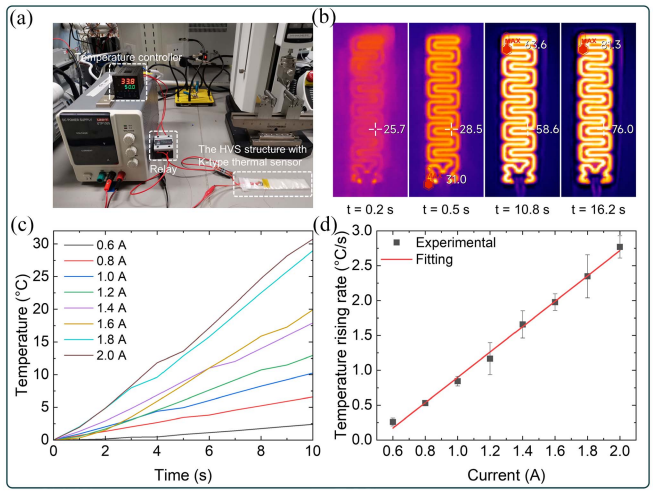

Fig. 6. Characterization of the heating/cooling efficiency of the HVS structure. (a) Experiment setup. (b) The infrared thermography during the heating process. (c) The temperature variation curves with different currents. (d) Temperature rising rate with different currents.

B. Hysteresis Characterization

Hysteresis (the residual deformation) refers to the path dependence of the HVS structure's force versus deformation. The hysteresis loops also offer vital information about the energy dissipated, which plays a pivotal role in the nonlinear modeling and the applicability of the HVS structure in soft robotic systems. The force-deflection curve obtained from the supplementary bending test (loading/unloading speed of 10 mm/min), can be used to analyze the hysteresis of the HVS structure. The experimental results (Fig. 4(a)) indicate that the hysteresis is minimal when the SMP exhibits elastic behavior at room temperature (25 °C) and without vacuum pressure. However, it amplifies with the rising temperature and the applied vacuum pressure. The origin of hysteresis of the HVS structure is attributed to the viscoelasticity of the SMP and the relative slippage between SMP layers during the jamming process. The hysteresis induced by vacuum pressure can be mitigated by closing the jamming system, while the hysteresis induced by the SMP can be effectively mitigated by the actuation of the soft robot under the low stiffness states. Therefore, the soft robots incorporating the HVS structure can efficiently recover to their initial configuration through the hybrid variable stiffness mechanism and the actuation system. The more comprehensive characterization of hysteretic behavior will be studied in future research.

C. FEA Simulation of the HVS Mechanism

The HVS structure undergoes large deformations that are challenging to analytically model. Finite element analysis (FEA) can recapitulate the mechanics computationally to generate quantitative data and provide an insightful understanding of the HVS's deformation behavior. Therefore, a three-dimensional (3D) and non-linear simulation was performed based on the ABAQUS/Explicit software package (Dassault Systèmes). The simulation model consists of two components: the HVS structure and the load device, while the element type utilized was the 8-node linear brick element (C3D8R), with a seed spacing of 0.3 mm as specified by the ABAQUS meshing algorithm. The geometric features and material properties were thoroughly considered to ensure consistency with the physical testing conditions. The bending device was specified as a rigid body to improve computational efficiency, where only contact between the HVS structure and the loading device was considered. A normal displacement with controllable amplitude was adopted to exert load.

The surface-to-surface contact with penalty friction formulation is adopted to simulate the contact behavior, including interlayer and the HVS structure to load device. The dynamic friction coefficients for contact are set based on the characterization of the tribological properties of SMP. The normal contact force between the load device and the HVS structure will be computed for further analysis. The simulation results of the HVS are shown in Fig. 5. The stress contour indicated that the stress increases with the deflection, as shown in Fig. 5(a). The force-deflection curve is shown in Fig. 5(b). The bending stiffness decreased from 12 N/mm to 4 N/mm with deflection increasing, which is caused by the interlayer slippage. The simulation results agree well with the experimental results, indicating the effectiveness of the simulation.

D. Investigation of the Response Time

To comprehensively investigate the response time of the HVS structure, a quantitative experimental study is undertaken, which encompasses two critical aspects: the heating/cooling efficiency of the SMP layer and the jamming response time, as shown in Fig. 6(a). The infrared thermography shows that the HVS structure has a uniform temperature distribution during the heating process, as shown in Fig. 6(b). The heating experiments were conducted under varying electrical currents I, ranging from 0.6 A

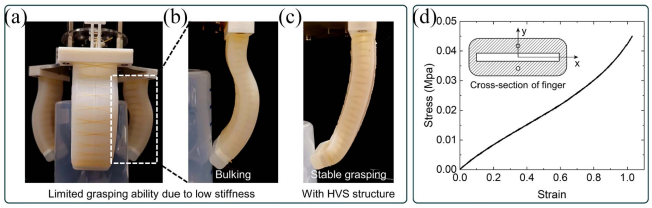

Fig. 7. Variable stiffness enhanced grasping ability. (a) (b) The instability and grasp failure due to low stiffness. (c) The enhanced grasping ability by HVS structure. (d) The stress-strain curve of silicone rubber.

to 2 A, as shown in Fig. 6(c). The heating power W is determined by the heating layer's resistance of R (11.5 ohms) and the current I. The maximum temperature rising rate is 2.77 ± 0.16 °C/s at 2 A, while the minimum temperature rising rate is 0.26 ± 0.06 °C/s at 0.6 A, as shown in Fig. 6(d). Compared to other MPT-based variable stiffness structures, the experimental results indicated that the proposed HVS structure can achieve a fast material phase transition, which is attributable to its unique sandwich configuration and slender layer composition. Correspondingly, cooling experiments were conducted under natural cooling at room temperature (25 °C), while the cooling rate (-0.14 ± 0.05 °C/s) was relatively low, considering there were no additional cooling equipment, which could be studied in future work to enhance the cooling efficiency. The jamming response is rapid, typically within milliseconds, due to the utilization of the vacuum pump with large power and the limited amount of air in the sealed bag.

Therefore, the proposed hybrid variable stiffness (HVS) mechanism integrates the intrinsic merits of the MPT-based and GR-based concepts (i.e., the SMP and LJ), which demonstrates the substantial potential for modulating bending stiffness and load-bearing capacity within a compact design and relatively fast response. Notably, in comparison to variable stiffness approaches exclusively based on SMP, the HVS structure can achieve a 1.60-fold stiffness enhancement within milliseconds, effectively reducing response time. Furthermore, compared to the layer jamming-based variable stiffness method, the HVS structure attained a remarkable 10-fold stiffness enhancement with merely 2 layers, effectively minimizing the volumetric demands of the jamming structure.

IV. The HVS Mechanism Enhanced Grasping Capability

The structural stiffness will significantly influence the compliance and the grasping capability of soft grippers. Grippers with low stiffness can conform to the object effectively due to its excellent compliance but may experience buckling instability as the driving force incrementally rises, which will restrict the force output capability and then lead to grasping failure, as shown in Fig. 7(a) and (b). In contrast, grippers with high stiffness can maintain structural stability under high driven force, enabling effective force transmission to the grasped object, thereby realizing larger force output and stable grasping capability, as shown in Fig. 7(c). Thus, an optimal balance between conformability for compliant grasping and high-force transmission for grasping heavy objects can be achieved by the proposed HVS structure.

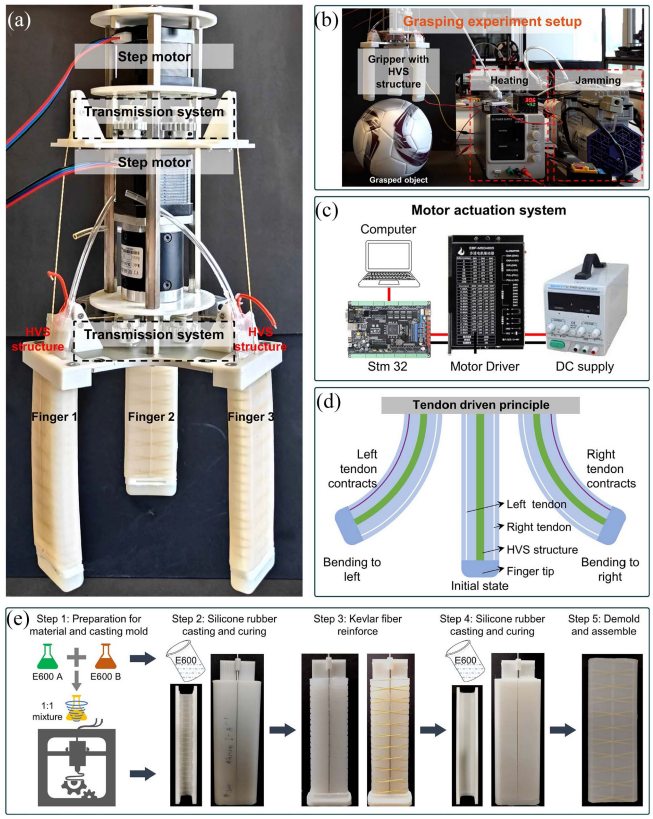

Fig. 8. Design, fabrication, and the tendon-driven principle of the soft gripper equipped with HVS structure. (a) Prototype of the variable stiffness soft gripper. (b) The grasping experiments platform. (c) The actuation system of the step motor. (d) The tendon-driven principle of the soft gripper. (e) The fabrication process of the fiber-reinforced soft finger.

The soft robotic gripper integrating the HVS structure was developed to fully characterize and validate the complex interplay between stiffness, morphology, and grasping ability, as shown in Fig. 8(a). The variable stiffness soft gripper comprises three articulated fingers at 120° intervals, which are secured to the base via screws. The HVS structure can be installed along the reserved holes of the fingers, which can be easily replaced with other variable stiffness or functional structures. Three HVS structures embedded in fingers are interconnected and integrated with the heating and jamming systems to achieve synchronous stiffness regulation during the grasping experiment, as shown in Fig. 8(b). The soft gripper implements a tendon-driven actuation mechanism. Each finger contains two eccentrically positioned driven tendons such that the contraction will generate a concentrated force and bending moment at the fingertip, which causes the finger to bend in different directions, as shown in Fig. 8(d). Tendon contraction is actuated by step motors (17HS8401, Hanpose Co., Ltd.), integrated with an actuation system comprising a STM32 controller (EmbedFire Co., Ltd.), and motor drivers (BH-MSD4805, EmbedFire Co., Ltd.), as shown in Fig. 8(c). The motor rotation is transferred to tendon contraction via the transmission system, which consists of an active gear coupled to the step motor shaft and three passive gears with the driven tendon wound. During the bending process of the gripper, the driven tendon is in close contact with the internal surface of the

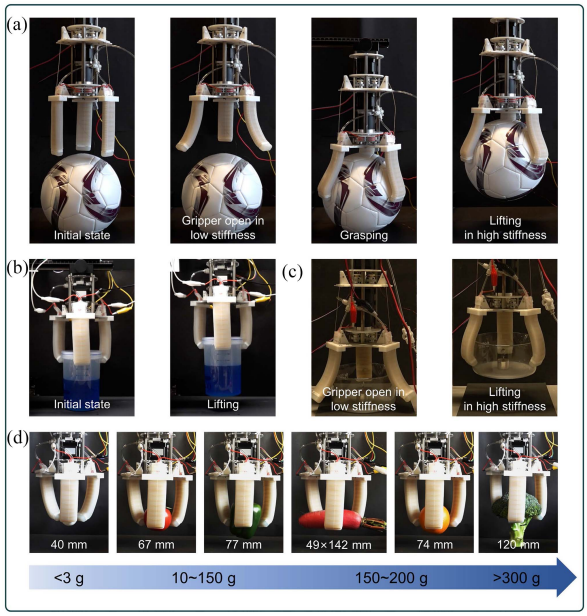

Fig. 9. HVS structure enhanced grasping capability of the soft gripper. (a) Grasping of a football (diameter ∼19.0 cm, weight ∼340 g). (b) Gripping of a cup of water (∼650 g). (c) Grasping of a glass tank (∼15.1 cm, ∼400 g). (d) Grasping of various fragile objects with shapes ranging from 40 mm to 120 mm, and weight ranging from 2.7 g to 300 g.

finger. Significant driven force is required to bend fingers in high stiffness, which may cause damage. To prevent this, soft fingers were reinforced with Kevlar fibers. The manufacturing process involves five steps, as shown in Fig. 8(e).

The bending stiffness of the soft finger is experimentally measured (0.20 ± 0.01 N/mm, Fig. 4(b)) and theoretically calculated using the formula $K = E{*}I$. The uniaxial tensile test results (Fig. 7(d)) indicate Young's modulus of the silicone rubber is approximately 0.038 MPa within a strain of 100%, and I_{Finger} is 10215 mm^4. The storage modulus of the SMP ranges from 1260 to 2.29 MPa between temperatures of 25 °C to 75 °C, and I_{HVS} is 3.33 mm^4 without vacuum pressure. Considering that I_{HVS} has a 1.60-fold increase due to vacuum pressure (Fig. 2), I_{HVS} is adjusted to 5.33 mm^4. Therefore, the calculated soft finger stiffness is 388.2 Mpa$*$mm^4. The theoretical stiffness of the HVS structure ranges from 6713.3 to 7.73 Mpa$*$mm^4. But it has been corrected to about 6713.3 to 427.6 Mpa$*$mm^4, based on the 15.7 times stiffness variable factor. Therefore, the HVS structure has a theoretical 17.3 to 1.10 stiffness ratio compared to the soft finger, which agrees well with the experimental results, indicating that the HVS structure can effectively adapt to the soft finger and can significantly enhance the structural stiffness without compromising the compliance of the soft robots.

The motions of the soft gripper embedded with the HVS structure have grasping and pinching, according to the different contact areas between the gripper and the objects. In the grasping motion illustrated by its interaction with large objects, such as a football (diameter ∼19 cm, weight ∼340 g) and a glass tank (∼15.1 cm, ∼400 g), the gripper's fingers make conformal contact with the grasped object's surface through its exceptional compliance. While in the pinching motion (a special grasping motion), such as lifting a weight cup, only the three fingertips will make simultaneous contact with the objects. The gripping process is as follows: First, the HVS structure is worked on State 1 and heated to 45°C to get low structural stiffness, enabling the gripper to open with minimal driven force. Next, the soft gripper is lowered and conforms to the object's contour. Subsequently, the HVS structure is switched to State 3 and cooled to increase stiffness. Finally, the gripper can grasp and lift the objects stably, as shown in Fig. 9(a) and (c). To demonstrate the grasping stability, versatility, and force output capability of the soft gripper with the HVS structure, several gripping experiments were also performed with different fragile objects, including table tennis ball, tomato, capsicum, carrot, orange, broccoli, and a cup of water. The HVS structure enabled the gripper to lift heavy loads, up to 650 g (Fig. 9(b)). The soft gripper has also shown great conformability to various shapes, including spherical, rod, and umbrella, with dimensions varying from 40 mm to 190 mm, and weights ranging from 2.7 g to 300 g, as shown in Fig. 9(d) and Supplementary Video S1.

V. Conclusion

This letter presents a hybrid variable stiffness (HVS) mechanism that integrates material phase transition (MPT)-based and geometric reconfiguration (GR)-based approaches (specifically utilizing shape memory polymer (SMP) and layer jamming (LJ)) to change stiffness. Stiffness is simultaneously modulated by modifying Young's modulus of the SMP layer through Joule heating and applying the vacuum pressure. To investigate the performance of the HVS mechanism, bending and response tests were performed. Bending test results revealed that the HVS structure can achieve a wide stiffness range (0.31 ± 0.013 N/mm $\sim$ 4.86 ± 0.11 N/mm, 15.7 times) and a wide range of load-bearing capacity (1.76 ± 0.21 N $\sim$ 28.1 ± 1.76 N, 16.0 times). Response test results showed that the jamming response is rapid (∼ms), and the maximum temperature rising rate is 2.77 ± 0.16 °C/s, indicating that the HVS structure can achieve a relatively fast response. Furthermore, a variable stiffness soft gripper was designed, and grasping experiments were conducted. The grasping tests showed the HVS structure can enhance the grasping abilities significantly, which enables the grasping of various objects with diverse shapes (40 mm $\sim$ 190 mm) and materials while lifting a weight up to 650 g, demonstrating its great potential for practical applications of soft robots. In future work, a barometer will be integrated into the jamming system for the continuous and precise control of vacuum pressure. More accurate analytical modeling of the HVS structure will also be studied.

Author Disclosure Statement: No competing financial interests exist.

Supplementary Material: Supplementary Video S1.

References

[1] D. Rus and M. T. Tolley, "Design, fabrication and control of soft robots," *Nature*, vol. 521, no. 7553, May 2015, Art. no. 7553, doi: 10.1038/nature14543.

[2] M. T. Tolley et al., "A resilient, untethered soft robot," *Soft Robot.*, vol. 1, no. 3, pp. 213–223, Sep. 2014, doi: 10.1089/soro.2014.0008.

[3] W. Yu et al., "A minimally-designed soft crawling robot for robust locomotion in unstructured pipes," *Bioinspiration Biomimetics*, vol. 17, 2022, Art. no. 056001, doi: 10.1088/1748-3190/ac7492.

[4] X. Li et al., "A mechanics model of hard-magnetic soft rod with deformable cross-section under three-dimensional large deformation," *Int. J. Solids Struct.*, vol. 279, May 2023, Art. no. 112344, doi: 10.1016/j.ijsolstr.2023.112344.

[5] E. T. Roche et al., "Soft robotic sleeve supports heart function," *Sci. Transl. Med.*, vol. 9, no. 373, Jan. 2017, Art. no. eaaf3925, doi: 10.1126/scitranslmed.aaf3925.

[6] P. Polygerinos, Z. Wang, K. C. Galloway, R. J. Wood, and C. J. Walsh, "Soft robotic glove for combined assistance and at-home rehabilitation," *Robot. Auton. Syst.*, vol. 73, pp. 135–143, Nov. 2015, doi: 10.1016/j.robot.2014.08.014.

[7] X. Li et al., "Geometrically exact finite element formulation for tendon-driven continuum robots," *Acta Mechanica Solida Sinica*, vol. 35, pp. 552–570, 2022, doi: 10.1007/s10338-022-00311-w.

[8] M. Cianchetti et al., "Soft robotics technologies to address shortcomings in today's minimally invasive surgery: The STIFF-FLOP approach," *Soft Robot*, vol. 1, no. 2, pp. 122–131, Jun. 2014, doi: 10.1089/soro.2014.0001.

[9] Y. S. Narang, J. J. Vlassak, and R. D. Howe, "Mechanically versatile soft machines through laminar jamming," *Adv. Funct. Mater.*, vol. 28, no. 17, 2018, Art. no. 1707136, doi: 10.1002/adfm.201707136.

[10] T. Wang, J. Zhang, Y. Li, J. Hong, and M. Y. Wang, "Electrostatic layer jamming variable stiffness for soft robotics," *IEEE/ASME Trans. Mechatron.*, vol. 24, no. 2, pp. 424–433, Apr. 2019, doi: 10.1109/TMECH.2019.2893480.

[11] X.-Y. Guo, W.-B. Li, Q.-H. Gao, H. Yan, Y.-Q. Fei, and W.-M. Zhang, "Self-locking mechanism for variable stiffness rigid–soft gripper," *Smart Mater. Struct.*, vol. 29, no. 3, 2020, Art. no. 035033, doi: 10.1088/1361-665X/ab710f.

[12] Y.-F. Zhang et al., "Fast-response, stiffness-tunable soft actuator by Hybrid Multimaterial 3D printing," *Adv. Funct. Mater.*, vol. 29, no. 15, 2019, Art. no. 1806698, doi: 10.1002/adfm.201806698.

[13] Q. Yu, M. Jiang, and N. Gravish, "Flexoskeleton fingers: 3D printed reconfigurable ridges enabling multi-functional and low-cost underactuated grasping," *IEEE Robot. Automat. Lett.*, vol. 6, no. 2, pp. 3971–3978, Apr. 2021, doi: 10.1109/LRA.2021.3067181.

[14] Y. S. Narang, A. Degirmenci, J. J. Vlassak, and R. D. Howe, "Transforming the dynamic response of robotic structures and systems through laminar jamming," *IEEE Robot. Automat. Lett.*, vol. 3, no. 2, pp. 688–695, Apr. 2018, doi: 10.1109/LRA.2017.2779802.

[15] A. Tonazzini, S. Mintchev, B. Schubert, B. Mazzolai, J. Shintake, and D. Floreano, "Variable stiffness Fiber with self-healing capability," *Adv. Mater.*, vol. 28, no. 46, pp. 10142–10148, 2016, doi: 10.1002/adma.201602580.

[16] M. Mattmann et al., "Thermoset shape memory polymer variable stiffness 4D robotic catheters," *Adv. Sci.*, vol. 9, no. 1, 2022, Art. no. 2103277, doi: 10.1002/advs.202103277.

[17] D. S. Shah, E. J. Yang, M. C. Yuen, E. C. Huang, and R. Kramer-Bottiglio, "Jamming skins that control system rigidity from the surface," *Adv. Funct. Mater.*, vol. 31, no. 1, 2021, Art. no. 2006915, doi: 10.1002/adfm.202006915.

[18] Y. Wang, L. Li, D. Hofmann, J. E. Andrade, and C. Daraio, "Structured fabrics with tunable mechanical properties," *Nature*, vol. 596, no. 7871, pp. 238–243, Aug. 2021, doi: 10.1038/s41586-021-03698-7.

[19] W. Wang and S.-H. Ahn, "Shape memory alloy-based soft gripper with variable stiffness for compliant and effective grasping," *Soft Robot.*, vol. 4, no. 4, pp. 379–389, Oct. 2017, doi: 10.1089/soro.2016.0081.

[20] J. Yan, Z. Xu, P. Shi, and J. Zhao, "A Human-inspired soft finger with dual-mode morphing enabled by variable stiffness mechanism," *Soft Robot.*, vol. 9, no. 2, pp. 399–411, Apr. 2022, doi: 10.1089/soro.2020.0153.

[21] R. A. Bilodeau, M. C. Yuen, and R. Kramer-Bottiglio, "Addressable, stretchable heating silicone sheets," *Adv. Mater. Technol.*, vol. 4, no. 9, 2019, Art. no. 1900276, doi: 10.1002/admt.201900276.

[22] Z. Yuan, L. Wu, X. Xu, and R. Chen, "Soft pneumatic gripper integrated with multi-configuration and variable-stiffness functionality," *Cogn. Computation Syst.*, vol. 3, no. 1, pp. 70–77, 2021, doi: 10.1049/ccs2.12009.

[23] D. Zhao et al., "A stiffness-switchable, biomimetic smart material enabled by supramolecular reconfiguration," *Adv. Mater.*, vol. 34, no. 10, 2022, Art. no. 2107857, doi: 10.1002/adma.202107857.

[24] X. Fang, J. Wen, L. Cheng, D. Yu, H. Zhang, and P. Gumbsch, "Programmable gear-based mechanical metamaterials," *Nature Mater.*, vol. 21, no. 8, pp. 869–876, Aug. 2022, doi: 10.1038/s41563-022-01269-3.

[25] X. Zhang, J. Yan, and J. Zhao, "A gas–Ribbon-hybrid actuated soft finger with active variable stiffness," *Soft Robot.*, vol. 9, pp. 250–265, 2021, doi: 10.1089/soro.2020.0031.

[26] Y. Jiang, D. Chen, C. Liu, and J. Li, "Chain-like granular jamming: A novel stiffness-programmable mechanism for soft robotics," *Soft Robot.*, vol. 6, no. 1, pp. 118–132, Feb. 2019, doi: 10.1089/soro.2018.0005.

[27] W. Park, D. Lee, and J. Bae, "A hybrid jamming structure combining granules and a chain structure for robotic applications," *Soft Robot.*, vol. 9, pp. 669–679, Jul. 2021, doi: 10.1089/soro.2020.0209.

[28] Y. Yang, Y. Zhang, Z. Kan, J. Zeng, and M. Y. Wang, "Hybrid jamming for bioinspired soft robotic fingers," *Soft Robot.*, vol. 7, no. 3, pp. 292–308, Jun. 2020, doi: 10.1089/soro.2019.0093.

[29] E. Brown et al., "Universal robotic gripper based on the jamming of granular material," *Proc. Nat. Acad. Sci.*, vol. 107, no. 44, pp. 18809–18814, Nov. 2010, doi: 10.1073/pnas.1003250107.

[30] S. Jadhav, M. R. A. Majit, B. Shih, J. P. Schulze, and M. T. Tolley, "Variable stiffness devices using Fiber jamming for application in soft robotics and wearable haptics," *Soft Robot.*, vol. 9, no. 1, pp. 173–186, 2022, doi: 10.1089/soro.2019.0203.

[31] M. Brancadoro, M. Manti, S. Tognarelli, and M. Cianchetti, "Preliminary experimental study on variable stiffness structures based on fiber jamming for soft robots," in *Proc. IEEE Int. Conf. Soft Robot.*, 2018, pp. 258–263, doi: 10.1109/ROBOSOFT.2018.8404929.

[32] F. Caruso, G. Mantriota, L. Afferrante, and G. Reina, "A theoretical model for multi-layer jamming systems," *Mechanism Mach. Theory*, vol. 172, Jun. 2022, Art. no. 104788, doi: 10.1016/j.mechmachtheory.2022.104788.

[33] Y.-J. Kim, S. Cheng, S. Kim, and K. Iagnemma, "A novel layer jamming mechanism with tunable stiffness capability for minimally invasive surgery," *IEEE Trans. Robot.*, vol. 29, no. 4, pp. 1031–1042, Aug. 2013, doi: 10.1109/TRO.2013.2256313.

[34] G. B. Crowley, X. Zeng, and H.-J. Su, "A 3D printed soft robotic gripper with a variable stiffness enabled by a novel positive pressure layer jamming technology," *IEEE Robot. Automat. Lett.*, vol. 7, no. 2, pp. 5477–5482, Apr. 2022, doi: 10.1109/LRA.2022.3157448.

[35] J.-Y. Lee et al., "Shape-adaptive universal soft parallel gripper for delicate grasping using a stiffness-variable composite structure," *IEEE Trans. Ind. Electron.*, vol. 68, no. 12, pp. 12441–12451, Dec. 2021, doi: 10.1109/TIE.2020.3044811.

[36] P. Wang, S. Guo, X. Wang, and Y. Wu, "Design and analysis of a novel variable stiffness continuum robot with built-in winding-styled ropes," *IEEE Robot. Automat. Lett.*, vol. 7, no. 3, pp. 6375–6382, Jul. 2022, doi: 10.1109/LRA.2022.3171917.

[37] Y. Pan, X.-J. Liu, and H. Zhao, "Stretchable and conformable variable stiffness device through an electrorheological fluid," *Soft Matter*, vol. 18, pp. 9163–9171, Nov. 2022, doi: 10.1039/D2SM01362B.

[38] C. Chautems, A. Tonazzini, D. Floreano, and B. J. Nelson, "A variable stiffness Catheter controlled with an external magnetic field," in *Proc. IEEE/RSJ Int. Conf. Intell. Robots Syst.*, 2017, pp. 181–186, doi: 10.1109/IROS.2017.8202155.

[39] I. M. Van Meerbeek et al., "Morphing metal and elastomer bicontinuous foams for reversible stiffness, shape memory, and self-healing soft machines," *Adv Mater*, vol. 28, no. 14, pp. 2801–2806, 2016, doi: 10.1002/adma.201505991.

[40] S. Park, N. Baugh, H. K. Shah, D. P. Parekh, I. D. Joshipura, and M. D. Dickey, "Ultrastretchable elastic shape memory fibers with electrical conductivity," *Adv. Sci.*, vol. 6, no. 21, 2019, Art. no. 1901579, doi: 10.1002/advs.201901579.

[41] T. T. Hoang, P. T. Phan, M. T. Thai, N. H. Lovell, and T. N. Do, "Bio-inspired conformable and helical soft fabric gripper with variable stiffness and touch sensing," *Adv. Mater. Technol.*, vol. 5, no. 12, 2020, Art. no. 2000724, doi: 10.1002/admt.202000724.

[42] T. T. Hoang, J. J. S. Quek, M. T. Thai, P. T. Phan, N. H. Lovell, and T. N. Do, "Soft robotic fabric gripper with gecko adhesion and variable stiffness," *Sensors Actuators A: Phys.*, vol. 323, Jun. 2021, Art. no. 112673, doi: 10.1016/j.sna.2021.112673.

[43] T. L. Buckner, E. L. White, M. C. Yuen, R. A. Bilodeau, and R. K. Kramer, "A move-and-hold pneumatic actuator enabled by self-softening variable stiffness materials," in *Proc. IEEE/RSJ Int. Conf. Intell. Robots Syst.*, 2017, pp. 3728–3733, doi: 10.1109/IROS.2017.8206221.

[44] L. Hines, V. Arabagi, and M. Sitti, "Shape memory polymer-based flexure stiffness control in a miniature flapping-wing robot," *IEEE Trans. Robot.*, vol. 28, no. 4, pp. 987–990, Aug. 2012, doi: 10.1109/TRO.2012.2197313.